Figure 1 *TUBB4A* mutations in patients with hypomyelinating leukoencephalopathy

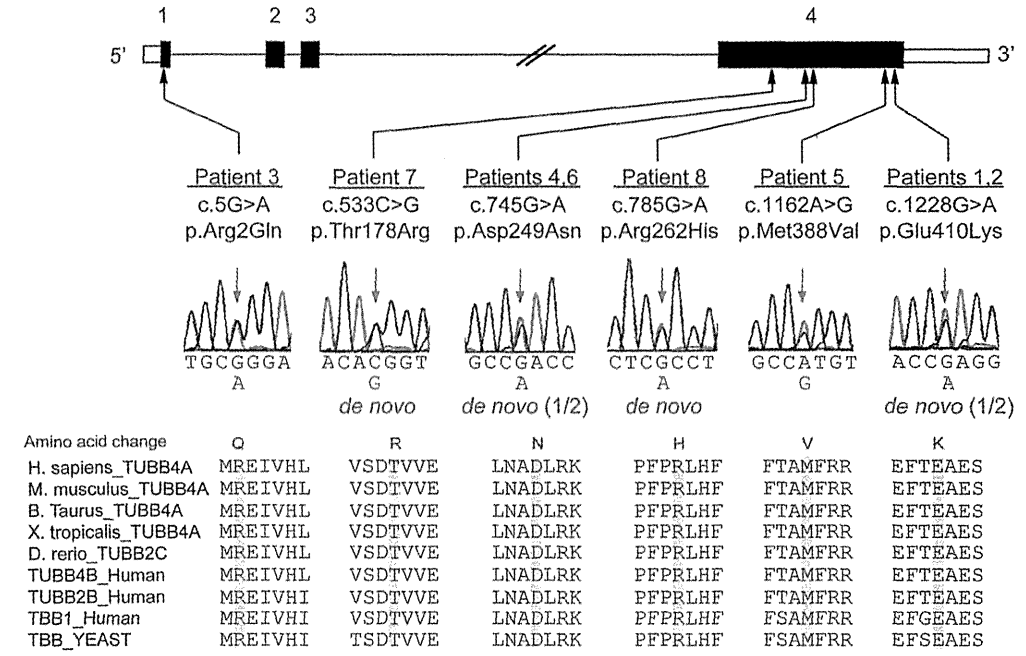

TUBB4A schematic with the 6 mutations is presented. Untranslated regions and coding regions are shown in white and black rectangles, respectively. All mutations occur at evolutionarily conserved amino acids. Homologous sequences were aligned using CLUSTALW (http://www.genome.jp/tools/clustalw/).

unsteady walking and others never acquiring head control. The maximum motor milestone of these patients was unstable short walking. The clinical course appeared milder in patients with an older age at onset. This tendency was most prominent in patients initially diagnosed with unclassified hypomyelinating leukoencephalopathy. For example, the onset of motor deterioration started in the first or second decades in these patients but was between 0 and 3 years old in patients with typical H-ABC. Intellectual disability was mild to moderate in the former but mostly severe in the latter patients.

All clinically evaluated patients with *TUBB4A* mutations demonstrated cerebellar ataxia and spasticity. Except for patient 8, all demonstrated extrapyramidal features such as rigidity, dystonia, or choreoathetosis. In patient 1, dystonia was prominent compared with other hypomyelination patients with either *POLR3A* or *POLR3B* mutations.[9,11] Patient 8 was 1 year old at the time of the study, and brain MRI showed a relatively small but still well-retained putamen compared with healthy subjects of the same age, suggesting that extrapyramidal features may not yet have developed but would likely express as the basal ganglia atrophy progressed. Notably, both hypomyelinating patients with either very mild basal ganglia atrophy (patient 2) or none identifiable (patient 1) demonstrated extrapyramidal signs, suggesting that the basal ganglia may be impaired functionally in these patients as well as other patients with typical H-ABC. Case reports are available in appendix e-1. Patients 1 and 2,[9] 4,[26] and 5[27] were previously described. Retrospectively, patient 2 might be diagnosed with atypical H-ABC because minimal basal ganglia atrophy cannot be excluded. In the patient with H-ABC with no *TUBB4A* mutation, the atrophy of basal ganglia was very mild compared with that of patients with typical H-ABC. However, clinical symptoms are very severe with neither head control nor sitting at 12 years, suggesting that the patient has atypical H-ABC.

DISCUSSION The β- and α-tubulins are major components of microtubules. Microtubules have essential roles in many cellular processes including mitosis, intracellular transport, asymmetric neuronal morphology, and ciliary and flagellar motility.[28] Multiple β-tubulin isotypes are present, with high homology (differing primarily at 15–20 amino acids within the C terminus), and expressed differentially in a tissue-dependent manner.[29] Certain isotypes, namely, β-tubulin isotypes 2A, 2B, 3, and 4A, are neuron-specific proteins and highly expressed in brain.[28] In the nervous system, microtubules provide structure, generate force necessary for neuronal migration, and serve as scaffolds for motor proteins and/or MAPs to transport cargo.[30] In addition to *TUBB4A*-associated leukoencephalopathies[17] and dystonia,[18,19] *TUBA1A*, *TUBB2B*, and *TUBB3*

© 2014 American Academy of Neurology. Unauthorized reproduction of this article is prohibited.

Figure 2 Structural prediction of *TUBB4A* mutations in the αβ-tubulin heterodimer

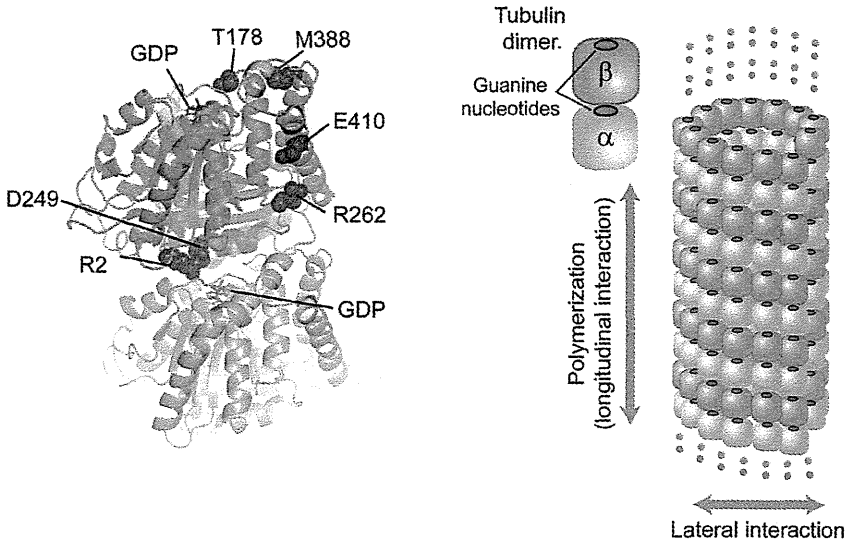

Mapping of disease-causing amino acid mutations on the αβ-tubulin heterodimer (Protein Data Bank code 1JFF) crystal structure, with schematic representation of a tubulin dimer (left) and microtubule segment (right). The α- and β-tubulins are colored gray and green, respectively. Left: The longitudinal interheterodimer interface of β-tubulin (which interacts with α-tubulin in a neighboring αβ heterodimer) is colored pink,[24] and the β-tubulin microtubule-associated protein and motor protein interaction region is colored cyan.[21,22] Side chains of residues altered by the mutations are shown in space-filling representation in red. Helices, β-sheets, and loops are shown as ribbons, arrows, and threads, respectively, and nucleotides are blue sticks. Right: Tubulin heterodimers polymerize longitudinally to form protofilaments (longitudinal interaction), then laterally interact with each other to form microtubules (lateral interaction). Blue circles represent guanine nucleotide–binding pockets of α- and β-tubulins.

mutations are reported to cause the spectrum of neurologic disorders resulting from neural migration, differentiation, and axon guidance and maintenance abnormalities,[25] demonstrating the importance of αβ-tubulin heterodimers in the nervous system.

In this study, we identified 6 missense *TUBB4A* mutations, 5 of which are novel, in 6 of 7 patients with H-ABC and 2 of 7 patients initially diagnosed with unclassified hypomyelinating leukoencephalopathy. Of the patients with H-ABC, all 6 patients with *TUBB4A* mutations showed typical H-ABC, supporting that H-ABC is a distinct disease entity caused by *TUBB4A* abnormality. We did not detect any *TUBB4A* mutations in one patient with atypical H-ABC. This may be because this patient has a clinically similar, but different disease, possibly caused by a different mutated gene.

We report a *TUBB4A* mutation in 2 patients with preserved basal ganglia. Their brain MRI findings are similar to patients with *POLR3A* or *POLR3B* mutations, rather than H-ABC. However, it is notable that both patients showed apparent extrapyramidal signs, to suggest functional impairment. Accompanying extrapyramidal features are extremely atypical in patients with either *POLR3A* or *POLR3B* mutations.[9,11] Furthermore, comparing these 2 patients with other typical H-ABC patients with *TUBB4A* mutations, patients with minimal basal ganglia atrophy tend to have a milder clinical course. Both patients have a recurrent missense mutation, c.1228G>A (p.Glu410Lys). Based on our 3-dimensional modeling analysis, the Glu410Lys mutation is predicted to directly impair motor protein and/or MAP interactions with microtubules, while the other mutations identified in patients with typical H-ABC may affect longitudinal interactions for maintaining αβ-tubulin heterodimerization/polymerization. Different effects of the *TUBB4A* mutations on tubulin function may lead to this phenotypic variation. Supporting this hypothesis, the p.Glu410Lys mutation in *TUBB3*, which also directly alters a kinesin motor protein binding site in β-tubulin isotype 3, demonstrates clinically distinct features compared with the other mutations.[30] Therefore, the p.Glu410Lys mutation in *TUBB4A* may contribute to the milder end of the phenotypic spectrum of *TUBB4A* mutations. Additional patients with *TUBB4A* mutations are needed to clinically confirm mutational consequences.

Another important finding is that one of the patients with H-ABC had a p.Arg2Gln mutation, since the p.Arg2Gly mutation has recently been identified in patients from a large DYT4 family.[18,19] DYT4 was described in 1985 in an Australian family that had emigrated from England as whispering dysphonia and generalized dystonia. To date, no other pedigrees

© 2014 American Academy of Neurology. Unauthorized reproduction of this article is prohibited.

Figure 3 Brain MRI of patients with *TUBB4A* mutations

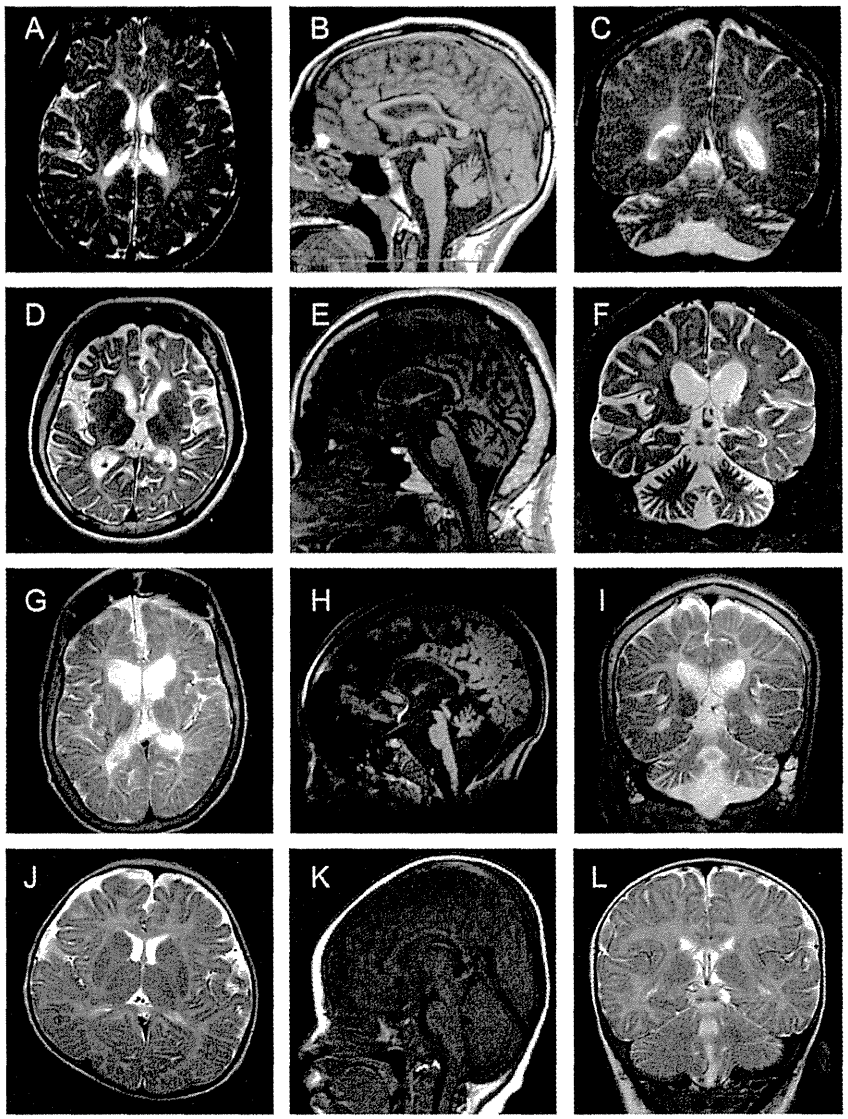

Axial T2-weighted (A, D, G, J), sagittal T1-weighted (B, E, H, K), and coronal T2-weighted (C, F, I, L) images. Patient 1 at 14 years of age (A); patient 1 at 16 years (B, C); patient 2 at 38 years (D–F); patient 3 at 13 years (G–I); and patient 8 at 7 months of age (J–L). All patients show diffuse cerebral white matter hypomyelination with normal (J), mildly reduced (A), or considerably reduced (D, G) white matter volumes. In patient 1, cerebral white matter hypomyelination is unchanged, comparing at 14 (A) and 16 (B, C) years of age. In patient 1, the putamen and the head of the caudate nucleus are normal in size (A). In patient 2, minimal putamen atrophy cannot be excluded (D). The putamen and the head of the caudate nucleus are small or hardly recognizable in patient 3 (G). In patient 8, the putamen is slightly small compared with a healthy control at the same age (J). The globus pallidus and thalamus are normal in size (A, D, G, J). Atrophy of the cerebellar vermis and hemisphere, and corpus callosum was variably observed in 4 patients, but not patient 8 (B, C, E, F, H, I, K, L).

with this phenotype have been reported worldwide.[18] The symptoms typically emerge in the third decade, following a highly penetrant, autosomal dominant mode of inheritance.[31] Brain MRI demonstrates normal structural findings. Arg2 resides within the autoregulatory MREI domain of β-tubulin 4A, which is necessary for autoregulation of the β-tubulin messenger RNA transcript. Site-directed mutagenesis shows that any Arg2 substitution leads to loss of autoregulated instability and increased mutant tubulin subunit levels.[32] Thus, mutations in the MREI domain have been assumed to cause DYT4 rather than H-ABC, because of the different impact on *TUBB4A*.[17] However, our study shows that mutations in the MREI domain can also cause the H-ABC phenotype. The phenotypic difference between the p.Arg2Gly and p.Arg2Gln mutations remains unsolved. Because DYT4 is an extremely rare

© 2014 American Academy of Neurology. Unauthorized reproduction of this article is prohibited.

syndrome that has only been described in one large pedigree so far, patients of the family may have another modifying factor(s) to spare cerebral white matter abnormalities.

Diffuse hypomyelination syndromes are a heterogeneous group of disorders with overlapping clinical features. Currently, they are categorized based on brain MRI findings, which is very useful in clinical practice. Basal ganglia atrophy specifically distinguishes H-ABC from other hypomyelination disorders. Our study shows that *TUBB4A* mutations associate not only with the typical H-ABC cases but also with some hypomyelinating patients with retained basal ganglia, although notably all patients with *TUBB4A* mutations have extrapyramidal features in common. Our study implies that *TUBB4A* may cause hypomyelinating leukoencephalopathies with either a morphologically or a functionally impaired basal ganglia. Extrapyramidal features may be a key for clinicians to examine *TUBB4A* mutations in genetically unsolved hypomyelinating leukoencephalopathies.

AUTHOR CONTRIBUTIONS

Satoko Miyatake: genetic and clinical data analysis, data interpretation, and drafting/revising of the manuscript. Hitoshi Osaka: clinical data analysis and sample collection. Masaaki Shiina: structural data analysis. Masayuki Sasaki, Jun-ichi Takanashi, Kazuhiro Haginoya, Takahito Wada, Masafumi Morimoto, Naoki Ando, and Yoji Ikuta: clinical data analysis and sample collection. Mitsuko Nakashima, Yoshinori Tsurusaki, and Noriko Miyake: genetic data analysis. Kazuhiro Ogata: structural data analysis. Naomichi Matsumoto: study concept and design, data interpretation, and drafting/revising of the manuscript. Hirotomo Saitsu: study concept and design, genetic data analysis, data interpretation, and drafting/revising of the manuscript.

ACKNOWLEDGMENT

The authors thank all of the participants for their cooperation in this research, and Dr. K. Nishiyama, Ms. K. Takabe, Mr. T. Miyama, Ms. A. Narita, Ms. N. Watanabe, and Ms. S. Sugimoto, from the Department of Human Genetics, Yokohama City University Graduate School of Medicine, for their technical assistance.

STUDY FUNDING

Supported by the Ministry of Health, Labour and Welfare of Japan; the Japan Society for the Promotion of Science (a Grant-in-Aid for Scientific Research [B] [25293085, 25293235]; and a Grant-in-Aid for Scientific Research [A] [13313587]); the Takeda Science Foundation; the fund for Creation of Innovation Centers for Advanced Interdisciplinary Research Areas Program in the Project for Developing Innovation Systems; the Strategic Research Program for Brain Sciences (11105137); and a Grant-in-Aid for Scientific Research on Innovative Areas (Transcription Cycle) from the Ministry of Education, Culture, Sports, Science and Technology of Japan (12024421).

DISCLOSURE

S. Miyatake is funded by research grants from the Yokohama Foundation for Advancement of Medical Science. H. Osaka is funded by research grants from the Ministry of Health, Labour and Welfare of Japan (Research on Rare and Intractable Diseases [H24-Nanchitou-Ippan-072]). M. Shiina and M. Sasaki report no disclosures relevant to the manuscript. J. Takanashi is funded by research grants from the Ministry of Health, Labour and Welfare of Japan (Research on Rare and Intractable Diseases [H24-Nanchitou-Ippan-072]). K. Haginoya, T. Wada, M. Morimoto, N. Ando, Y. Ikuta, M. Nakashima, and Y. Tsurusaki report no disclosures relevant to the manuscript. N. Miyake is funded by research grants from the Ministry of Health, Labour and Welfare of Japan, a Grant-in-Aid for Scientific Research (B) from the Japan Society for the Promotion of Science, and a research grant from the Takeda Science Foundation. K. Ogata is supported by a Grant-in-Aid for Scientific Research on Innovative Areas (Transcription Cycle) from the Ministry of Education, Culture, Sports, Science and Technology of Japan. N. Matsumoto is supported by grants from the Ministry of Health, Labour and Welfare of Japan, a Grant-in-Aid for Scientific Research (A) from the Japan Society for the Promotion of Science, the Takeda Science Foundation, the fund for Creation of Innovation Centers for Advanced Interdisciplinary Research Areas Program in the Project for Developing Innovation Systems, the Strategic Research Program for Brain Sciences, and a Grant-in-Aid for Scientific Research on Innovative Areas (Transcription Cycle) from the Ministry of Education, Culture, Sports, Science and Technology of Japan. H. Saitsu is funded by research grants from a Grant-in-Aid for Scientific Research (B) from the Japan Society for the Promotion of Science, and a research grant from the Takeda Science Foundation. Go to Neurology.org for full disclosures.

Received October 10, 2013. Accepted in final form March 20, 2014.

REFERENCES

1. Schiffmann R, van der Knaap MS. Invited article: an MRI-based approach to the diagnosis of white matter disorders. Neurology 2009;72:750–759.
2. Steenweg ME, Vanderver A, Blaser S, et al. Magnetic resonance imaging pattern recognition in hypomyelinating disorders. Brain 2010;133:2971–2982.
3. Wolf NI, Harting I, Boltshauser E, et al. Leukoencephalopathy with ataxia, hypodontia, and hypomyelination. Neurology 2005;64:1461–1464.
4. Timmons M, Tsokos M, Asab MA, et al. Peripheral and central hypomyelination with hypogonadotropic hypogonadism and hypodontia. Neurology 2006;67:2066–2069.
5. Vazquez-Lopez M, Ruiz-Martin Y, de Castro-Castro P, Garzo-Fernandez C, Martin-del Valle F, Marquez-de la Plata L. Central hypomyelination, hypogonadotrophic hypogonadism and hypodontia: a new leukodystrophy [in Spanish]. Rev Neurol 2008;47:204–208.
6. Bernard G, Thiffault I, Tetreault M, et al. Tremor-ataxia with central hypomyelination (TACH) leukodystrophy maps to chromosome 10q22.3-10q23.31. Neurogenetics 2010;11:457–464.
7. Atrouni S, Daraze A, Tamraz J, Cassia A, Caillaud C, Megarbane A. Leukodystrophy associated with oligodontia in a large inbred family: fortuitous association or new entity? Am J Med Genet A 2003;118A:76–81.
8. Chouery E, Delague V, Jalkh N, et al. A whole-genome scan in a large family with leukodystrophy and oligodontia reveals linkage to 10q22. Neurogenetics 2011;12:73–78.
9. Sasaki M, Takanashi J, Tada H, Sakuma H, Furushima W, Sato N. Diffuse cerebral hypomyelination with cerebellar atrophy and hypoplasia of the corpus callosum. Brain Dev 2009;31:582–587.
10. Bernard G, Chouery E, Putorti ML, et al. Mutations of POLR3A encoding a catalytic subunit of RNA polymerase Pol III cause a recessive hypomyelinating leukodystrophy. Am J Hum Genet 2011;89:415–423.
11. Saitsu H, Osaka H, Sasaki M, et al. Mutations in POLR3A and POLR3B encoding RNA polymerase III subunits cause an autosomal-recessive hypomyelinating leukoencephalopathy. Am J Hum Genet 2011;89:644–651.
12. Tetreault M, Choquet K, Orcesi S, et al. Recessive mutations in POLR3B, encoding the second largest subunit of Pol III, cause a rare hypomyelinating leukodystrophy. Am J Hum Genet 2011;89:652–655.

© 2014 American Academy of Neurology. Unauthorized reproduction of this article is prohibited.

13. Poric A, Brais B, Choquet K, Schiffmann R, Bernard G. 4H syndrome with late-onset growth hormone deficiency caused by POLR3A mutations. Arch Neurol 2012;69: 920–923.
14. Daoud H, Tetreault M, Gibson W, et al. Mutations in POLR3A and POLR3B are a major cause of hypomyelinating leukodystrophies with or without dental abnormalities and/or hypogonadotropic hypogonadism. J Med Genet 2013;50:194–197.
15. van der Knaap MS, Naidu S, Pouwels PJ, et al. New syndrome characterized by hypomyelination with atrophy of the basal ganglia and cerebellum. AJNR Am J Neuroradiol 2002;23:1466–1474.
16. van der Knaap MS, Linnankivi T, Paetau A, et al. Hypomyelination with atrophy of the basal ganglia and cerebellum: follow-up and pathology. Neurology 2007;69: 166–171.
17. Simons C, Wolf NI, McNeil N, et al. A de novo mutation in the beta-tubulin gene TUBB4A results in the leukoencephalopathy hypomyelination with atrophy of the basal ganglia and cerebellum. Am J Hum Genet 2013;92: 767–773.
18. Hersheson J, Mencacci NE, Davis M, et al. Mutations in the autoregulatory domain of beta-tubulin 4a cause hereditary dystonia. Ann Neurol 2013;73:546–553.
19. Lohmann K, Wilcox RA, Winkler S, et al. Whispering dysphonia (DYT4 dystonia) is caused by a mutation in the TUBB4 gene. Ann Neurol 2013;73:537–545.
20. Lowe J, Li H, Downing KH, Nogales E. Refined structure of alpha beta-tubulin at 3.5 Å resolution. J Mol Biol 2001; 313:1045–1057.
21. Uchimura S, Oguchi Y, Katsuki M, et al. Identification of a strong binding site for kinesin on the microtubule using mutant analysis of tubulin. EMBO J 2006;25:5932–5941.
22. Al-Bassam J, Ozer RS, Safer D, Halpain S, Milligan RA. MAP2 and tau bind longitudinally along the outer ridges of microtubule protofilaments. J Cell Biol 2002;157: 1187–1196.
23. Nawrotek A, Knossow M, Gigant B. The determinants that govern microtubule assembly from the atomic structure of GTP-tubulin. J Mol Biol 2011;412:35–42.
24. Nogales E, Whittaker M, Milligan RA, Downing KH. High-resolution model of the microtubule. Cell 1999; 96:79–88.
25. Tischfield MA, Cederquist GY, Gupta ML Jr, Engle EC. Phenotypic spectrum of the tubulin-related disorders and functional implications of disease-causing mutations. Curr Opin Genet Dev 2011;21:286–294.
26. Wakusawa K, Haginoya K, Kitamura T, et al. Effective treatment with levodopa and carbidopa for hypomyelination with atrophy of the basal ganglia and cerebellum. Tohoku J Exp Med 2006;209:163–167.
27. Hattori A, Ando N, Fujimoto S, Kobayashi S, Ishikawa T, Togari H. A boy with hypomyelination with atrophy of the basal ganglia and cerebellum [in Japanese]. No To Hattatsu 2010;42:42–44.
28. Leandro-Garcia LJ, Leskela S, Landa I, et al. Tumoral and tissue-specific expression of the major human beta-tubulin isotypes. Cytoskeleton 2010;67:214–223.
29. Sullivan KF, Cleveland DW. Sequence of a highly divergent beta tubulin gene reveals regional heterogeneity in the beta tubulin polypeptide. J Cell Biol 1984;99:1754–1760.
30. Chew S, Balasubramanian R, Chan WM, et al. A novel syndrome caused by the E410K amino acid substitution in the neuronal beta-tubulin isotype 3. Brain 2013;136: 522–535.
31. Parker N. Hereditary whispering dysphonia. J Neurol Neurosurg Psychiatry 1985;48:218–224.
32. Yen TJ, Machlin PS, Cleveland DW. Autoregulated instability of beta-tubulin mRNAs by recognition of the nascent amino terminus of beta-tubulin. Nature 1988;334: 580–585.

Enjoy Big Savings on NEW 2014 AAN Practice Management Webinars Subscriptions

The American Academy of Neurology offers 14 cost-effective Practice Management Webinars you can attend live or listen to recordings posted online. AAN members can purchase one webinar for $149 or subscribe to the entire series for only $199. *This is new pricing for 2014 and significantly less than 2013*—and big savings from the new 2014 nonmember price of $199 per webinar or $649 for the subscription. Register today for these and other 2014 webinars at *AAN.com/view/pmw14*:

April 8 – How PQRS Quality Measures Will Inform Future Medicare Value-based Payments

May 13 – Measuring and Improving Your Patients' Experience

June 18 – Using Practice Benchmarking Analytics to Improve Your Bottom Line

© 2014 American Academy of Neurology. Unauthorized reproduction of this article is prohibited.

PIGA mutations cause early-onset epileptic encephalopathies and distinctive features

Mitsuhiro Kato, MD, PhD*
Hirotomo Saitsu, MD, PhD*
Yoshiko Murakami, MD, PhD*
Kenjiro Kikuchi, MD
Shuei Watanabe, MD
Mizue Iai, MD
Kazushi Miya, MD
Ryuki Matsuura, MD
Rumiko Takayama, MD
Chihiro Ohba, MD
Mitsuko Nakashima, MD, PhD
Yoshinori Tsurusaki, PhD
Noriko Miyake, MD, PhD
Shin-ichiro Hamano, MD
Hitoshi Osaka, MD, PhD
Kiyoshi Hayasaka, MD, PhD
Taroh Kinoshita, PhD
Naomichi Matsumoto, MD, PhD

Correspondence to
Dr. Kato:
mkato@med.id.yamagata-u.ac.jp
or Dr. Saitsu:
hsaitsu@yokohama-cu.ac.jp

ABSTRACT

Objective: To investigate the clinical spectrum caused by mutations in *PIGA* at Xp22.2, which is involved in the biosynthesis of the glycosylphosphatidylinositol (GPI) anchor, among patients with early-onset epileptic encephalopathies (EOEEs).

Methods: Whole-exome sequencing was performed as a comprehensive genetic analysis for a cohort of 172 patients with EOEEs including early myoclonic encephalopathy, Ohtahara syndrome, and West syndrome, and *PIGA* mutations were carefully investigated.

Results: We identified 4 *PIGA* mutations in probands showing early myoclonic encephalopathy, West syndrome, or unclassified EOEE. Flow cytometry of blood granulocytes from patients demonstrated reduced expression of GPI-anchored proteins. Expression of GPI-anchored proteins in *PIGA*-deficient JY5 cells was only partially or hardly restored by transient expression of PIGA mutants with a weak TATA box promoter, indicating a variable loss of PIGA activity. The phenotypic consequences of *PIGA* mutations can be classified into 2 types, severe and less severe, which correlate with the degree of PIGA activity reduction caused by the mutations. Severe forms involved myoclonus and asymmetrical suppression bursts on EEG, multiple anomalies with a dysmorphic face, and delayed myelination with restricted diffusion patterns in specific areas. The less severe form presented with intellectual disability and treatable seizures without facial dysmorphism.

Conclusions: Our study confirmed that *PIGA* mutations are one genetic cause of EOEE, suggesting that GPI-anchor deficiencies may be an underlying cause of EOEE. ***Neurology*® 2014;82:1587–1596**

GLOSSARY

ADC = apparent diffusion coefficient; **cDNA** = complementary DNA; **DWI** = diffusion-weighted image; **EME** = early myoclonic encephalopathy; **EOEE** = early-onset epileptic encephalopathy; **GPI** = glycosylphosphatidylinositol; **GPI-AP** = glycosylphosphatidylinositol-anchored protein; **OS** = Ohtahara syndrome; **WES** = whole-exome sequencing.

Early-onset epileptic encephalopathies (EOEEs) present with developmental impairment and disastrous seizures starting in early infancy with a mode of age dependency. Ohtahara syndrome (OS) and early myoclonic encephalopathy (EME), both of which show a distinctive EEG finding called suppression-burst pattern, are neonatal EOEEs. Genetic approaches have revealed some of the genes that are mutated in EOEEs. For instance, *ARX*, *STXBP1*, *CASK*, *KCNQ2*, and *SCN2A* are mutated in OS,[1–5] while *ARX*, *CDKL5*, and *SPTAN1* mutations cause West syndrome or infantile spasms.[6–8]

Mutations in 8 genes (*PIGA*, *PIGM*, *PIGN*, *PIGV*, *PIGL*, *PIGO*, *PIGT*, and *PGAP2*) involved in the biosynthesis of the glycosylphosphatidylinositol (GPI) anchor, a glycolipid structure embedded in the plasma membrane that attaches to hundreds of cell-surface proteins, have been identified in patients with a variety of multiple congenital anomalies, intellectual disability, and epileptic seizures.[9–16] Somatic mutations of *PIGA* at Xp22.2, which is involved in

Supplemental data at Neurology.org

*These authors contributed equally to this work.

From the Department of Pediatrics (M.K., K.H.), Yamagata University Faculty of Medicine, Yamagata; Department of Human Genetics (H.S., C.O., M.N., Y.T., N. Miyake, N. Matsumoto), Yokohama City University Graduate School of Medicine, Yokohama; Department of Immunoregulation (Y.M., T.K.), Research Institute for Microbial Diseases, and WPI Immunology Frontier Research Center, Osaka University, Suita; Division of Neurology (K.K., R.M., S.-i.H.), Saitama Children's Medical Center, Saitama; Division of Neurology (S.W.), Miyagi Children's Hospital, Sendai; Division of Neurology (M.I., H.O.), Clinical Research Institute, Kanagawa Children's Medical Center, Yokohama; Department of Pediatrics (K.M.), Graduate School of Medicine and Pharmaceutical Sciences, University of Toyama; Department of Pediatrics (R.T.), Aomori Prefectural Central Hospital, Aomori; and Department of Pediatrics (H.O.), Jichi Medical School, Tochigi, Japan.

Go to Neurology.org for full disclosures. Funding information and disclosures deemed relevant by the authors, if any, are provided at the end of the article.

© 2014 American Academy of Neurology

© 2014 American Academy of Neurology. Unauthorized reproduction of this article is prohibited.

the first step of the GPI biosynthesis, are responsible for paroxysmal nocturnal hemoglobinuria, and its germline mutation, were recently identified in a family with multiple congenital anomalies, neonatal seizures, and a poor prognosis.[11] At least 2 of 3 patients in this family showed severe myoclonic seizures with suppression bursts on EEG, strongly suggesting EME. The known mutations in EME prompted us to investigate *PIGA* in the EOEE patient cohort including EME and OS. We identified *PIGA* mutations in 5 patients from 4 families with EOEEs and present the clinical phenotypes of the patients and functional effects of the mutations in this study.

METHODS

Patients. A total of 172 patients with EOEEs (2 with EME, 50 with OS, 50 with West syndrome or infantile spasms, 7 with malignant migrating partial seizures in infancy, and 63 with unclassified epileptic encephalopathy with an age at onset of <1 year; 90 male and 82 female patients) were analyzed by whole-exome sequencing (WES), and *PIGA* mutations were carefully investigated using WES data.

Patients had been mainly enrolled in the Japanese collaborative study for EOEE since 2003. The diagnosis was made based on clinical features and characteristic EEG patterns. Patients with mutations in *STXBP1, ARX, KCNQ2, SCN1A, SCN2A, KCNT1, CDKL5, CASK,* or *MECP2,* which were detected by high-resolution melting analysis, target capture analysis, direct sequencing analysis, or WES, were excluded from the study.

Whole-exome sequencing. Patient and parental genomic DNA was obtained from peripheral blood leukocytes using standard methods. DNA was captured using the SureSelectXT Human All Exon Kit (v4 or v5; Agilent Technologies, Santa Clara, CA) and sequenced on an Illumina HiSeq2000 (Illumina, San Diego, CA) with 101–base pair paired-end reads. Image analysis and base calling were performed using sequence control software real-time analysis and CASAVA software v1.8 (Illumina). Exome data processing, variant calling, and variant annotation were performed as previously described.[17–19] All novel mutations in *PIGA* were verified using Sanger sequencing.

Fluorescence-activated cell sorting analysis. Surface expression of GPI-anchored proteins (GPI-APs) was determined by staining cells with Alexa 488–conjugated inactivated aerolysin (FLAER; Protox Biotech, Victoria, Canada) and appropriate primary antibodies, namely, mouse anti-CD59 (5H8), DAF (IA10), CD16 (3G8), CD24 (ML5), and CD48 (BJ40), followed by a phycoerythrin-conjugated anti-mouse immunoglobulin G antibody (3G8, ML5, BJ40, and secondary antibodies; BD Biosciences, Franklin Lakes, NJ). Cells were analyzed by flow cytometry (Cant II; BD Biosciences).

Functional analysis using *PIGA*-deficient B lymphoblastoid cells (JY5). FLAG-tagged human *PIGA* complementary DNA (cDNA) and mutant cDNAs, generated by site-directed mutagenesis, were subcloned into the pMEoriP vector, a strong promoter (SRα)-driven vector or pTAoriP, a weak TATA box promoter-driven vector. Plasmid DNA was transfected by electroporation into *PIGA*-deficient JY5 cells. Expression of GPI-APs was analyzed by fluorescence-activated cell sorting. PIGA protein levels in transfected cells were determined by Western blotting using an anti-FLAG antibody (M2; Sigma, St. Louis, MO).

Standard protocol approvals, registrations, and patient consents. The experimental protocols were approved by the institutional review boards for ethical issues of Yamagata University Faculty of Medicine, Yokohama City University School of Medicine, and Osaka University, Japan. Written informed consent was obtained from all individuals and/or their families in compliance with relevant Japanese regulations. Permission for publishing photographs was also obtained from the parents.

RESULTS

Identification of *PIGA* mutations. No mutations were found in *SLC25A22*, which had been reported in a family of EME.[20] We identified 4 hemizygous *PIGA* mutations in 3 sporadic patients and 2 siblings with EOEE. One mutation (c.1234C>T [p.R412X]) had previously been reported,[11] while the other 3 were novel missense mutations (c.230G>T [p.R77L], c.616A>T [p.I206F], and c.355C>T [p.R119W]). DNA from the mother of patient 1 (p.R412X) was unavailable. Three missense mutations were maternally inherited. All mutations were absent from the 6,500 exomes of the National Heart, Lung, and Blood Institute exome project and our 573 in-house control exomes (281 male and 292 female patients). All 4 mutations occurred at evolutionarily conserved amino acids (figure 1A) and were predicted to be highly damaging to the protein structure by SIFT, PolyPhen-2, and MutationTaster (table e-1 on the *Neurology*® Web site at Neurology.org), which supported their pathogenicity.

Clinical features of patients with the *PIGA* mutation. The clinical information of individuals with a *PIGA* mutation is summarized in table 1, and their facial appearances and representative brain images are shown in figures 1 and 2, respectively. EEG findings (figure e-1) and detailed case reports (appendix e-1) are available in supplemental data. Two patients were associated with polyhydramnios. Birth weight and length were normal in 3 patients (patients 2, 3, and 5) who were born at term, but the other 2 who were born at preterm showed higher (patient 1) or lower (patient 4) birth weights than normal. Three patients with the severe phenotype (patients 1, 2, and 5) showed facial dysmorphisms (figure 1, B and C), including a depressed nasal bridge, short anteverted nose, downturned corners of the mouth, and high arched palate. Patient 1 also showed bilateral vesicoureteral reflux of the most severe grade V. In addition, brain MRI demonstrated a thin corpus callosum and delayed myelination in these patients. Of interest, abnormally high signals on diffusion-weighted images (DWIs) and low signals on the apparent diffusion coefficient (ADC) map at the brainstem, basal ganglia, thalamus, and deep white matter were found in patients 1, 2, and 5 (figure 2, A–D and M–Q). By

© 2014 American Academy of Neurology. Unauthorized reproduction of this article is prohibited.

Figure 1 *PIGA* mutations in patients with epileptic encephalopathy and dysmorphic features

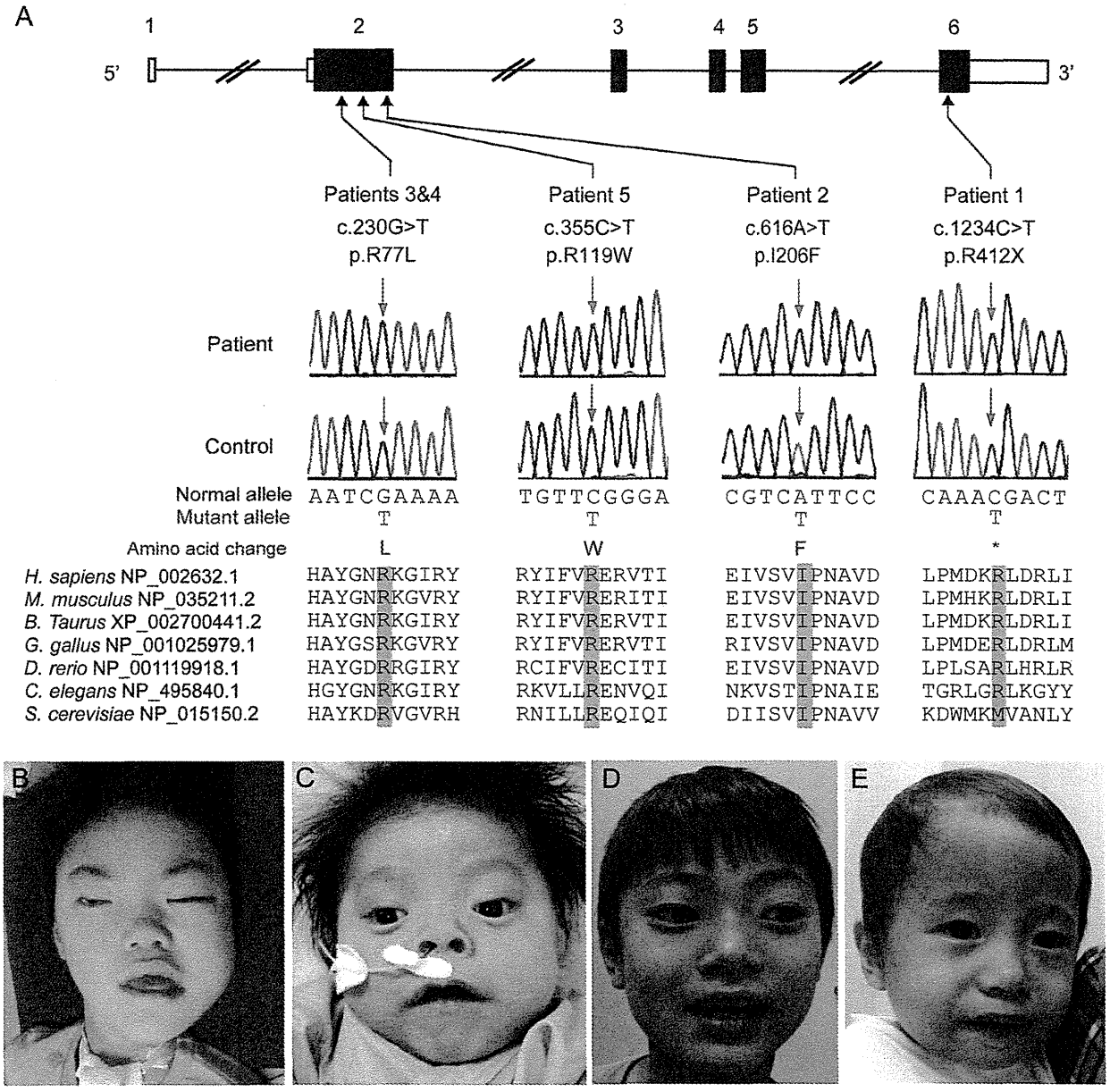

(A) Schematic presentation of *PIGA* genomic structure. Mutations are indicated based on the transcript variant 1 (GenBank accession number, NM_002641.3). Untranslated regions and coding regions are shown as white and black rectangles, respectively. All mutations occurred at evolutionarily conserved amino acids. Orthologous sequences were aligned using the CLUSTALW Web site. (B–E) Facial appearance of patients 2, 3, 4, and 5. Both patients 2 (B) and 5 (C) show distinct facial features, such as upslanting palpebral fissures, depressed nasal bridge, short anteverted nose, triangular mouth with downturned corners, and high arched palate, compared with patients 3 (D) and 4 (E) with no dysmorphic facial features.

contrast, 2 brothers with a less severe phenotype (patients 3 and 4) showed neither dysmorphic signs nor abnormalities in brain MRI (figure 2, E–L).

The first seizures started between 1 and 7 months of age, and tonic or myoclonic seizures occurred in all patients. Seizures of patients 1, 2, and 5 were refractory to antiepileptic medications, but topiramate was effective for the seizures of patient 3. The initial EEG showed a suppression burst in patient 1; patients 2 and 5 first demonstrated hypsarrhythmia, followed by a symmetrical or asymmetrical suppression burst later (figure e-1). Serum alkaline phosphatase levels were elevated in patients 2 and 5. No patients showed anemia or hemoglobinuria. All patients showed profound intellectual disability, and patients 1, 2, and 5 were bedridden with severe motor disturbance.

Flow cytometry. We analyzed the surface expression of various GPI-APs on patient granulocytes using flow

© 2014 American Academy of Neurology. Unauthorized reproduction of this article is prohibited.

Neurology 82 May 6, 2014

Table 1 Clinical summary of patients with a *PIGA* mutation

	Patients						
	IV-2	IV-4	1	2	3	4	5
Familial or sporadic	Familial or sporadic	Familial (brother)	Sporadic	Sporadic	Familial (proband)	Familial (brother)	Sporadic
Mutation	c.1234C>T (p.R412X)	c.1234C>T (p.R412X)	c.1234C>T (p.R412X)	c.616A>T (p.I206F)	c.230G>T (p.R77L)	c.230G>T (p.R77L)	c.355C>T (p.R119W)
Current age	Died at 11 wk	Died at 10 wk	6 y	10 y	8 y	18 mo	15 mo
Sex	M	M	M	M	M	M	M
Clinical diagnosis			Ohtahara syndrome, early myoclonic encephalopathy, Schinzel-Giedion syndrome	West syndrome with hypomyelination	Early-onset epileptic encephalopathy	Early-onset epileptic encephalopathy	West syndrome
Polyhydramnios	–	+	+	–	–	–	+
Gestation, wk	Full term	35	33	40	38	36	39
Birth weight, g	3,540	3,500	2,857	3,566	2,715	1,896	3,468
Birth length, cm	53.5	48	42.0	50	50	ND	47
Birth head circumference, cm	37	35.5	33.2	ND	32.5	ND	33.5
Facial dysmorphism	+	+	+	+	–	–	+
Vesicoureteral reflux	+	ND	+	ND	–	–	ND
Joint contractures	+	+	+	+	–	–	–
Hypotonia	+	+	+	–	–	–	+
Hyperreflexia	+	+	ND	–	–	–	+
Seizure onset	Neonate	Neonate	1 mo	3 mo	7 mo	7 mo	3 mo
Seizure types	Myoclonic	Severe myoclonic	Tonic seizures followed by frequent myoclonus	Myoclonus or epileptic spasm-like movement	Tonic seizures, secondarily generalized seizures	Tonic or clonic	Myoclonic seizures, tonic spasms
EEG findings	Suppression burst	Suppression burst	Suppression burst at neonatal period	Hypsarrhythmia at 3 mo, periodic bursts of multifocal epileptic discharges similar to suppression-burst pattern at 10 y	Normal at 7 mo, irregular spike and slow wave and multifocal spikes at 2 and 5 y	Normal at 7 mo	Hypsarrhythmia at 3 mo, suppression burst at 5 mo
Seizure prognosis	Intractable	Intractable	Intractable	Intractable	Seizure-free at 3 y with TPM	Seizure-free at 15 mo	Intractable
Development	Early death	Early death	Hypotonic quadriplegia, profound intellectual disability	Spastic quadriplegia, profound intellectual disability	Profound intellectual disability with autism, but no motor disturbance	Moderate intellectual disability, but no motor disturbance	Hypotonic quadriplegia, profound intellectual disability
Thin corpus callosum	+	+	+	+	–	–	+ (at 9 mo)
White matter immaturity	+	+	+	+	–	–	+ (at 9 mo)
Restricted diffusion pattern	ND	ND	+	+	–	–	+
Elevated serum alkaline phosphatase	ND	+	ND	+	–	–	+

Abbreviations: ND = not determined; TPM = topiramate.

© 2014 American Academy of Neurology. Unauthorized reproduction of this article is prohibited.

Figure 2 Brain MRIs of patients with *PIGA* mutations

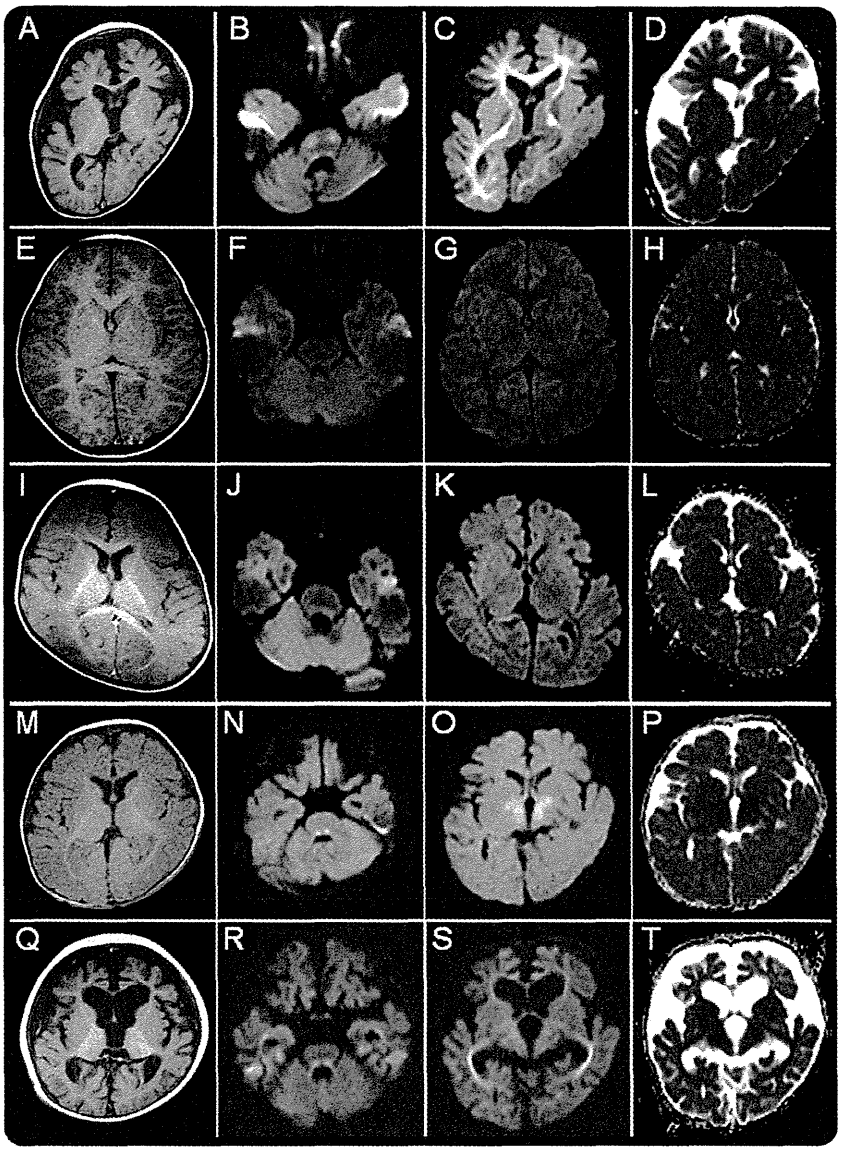

MRIs of patient 2 at 6 months (A) and 7 years (B–D), patient 3 at 3 years (E–H), patient 4 at 7 months (I–L), and patient 5 at 3 months (M–P) and 9 months (Q–T) of age. Left panels (A, E, I, M, Q) show axial T1-weighted images, the 2 middle panels (B, C, F, G, J, K, N, O, R, S) show axial diffusion-weighted images (DWIs), and right panels (D, H, L, P, T) show apparent diffusion coefficient (ADC) maps. Patient 2 and patient 5 at 9 months show cortical atrophy and enlarged ventricles. Note the high signals on DWI in the pontine tegmentum and deep white matter, particularly the optic radiation, of patients 2 and 5 in accordance with their age. The ADC map demonstrated decreased ADC within the same lesion. Patients 3 and 4 show normal images.

cytometry (figure 3). In all 5 patients, the surface expression of CD16 was severely decreased (from 5% to 15% of normal levels). Patient 1, with the most severe clinical symptoms, had a tendency to show reduced expression of other GPI-APs, such as CD24 and FLAER (figure 4A). Because *PIGA* is an X-linked gene and one allele is inactivated during early embryogenesis in female patients, patient mothers would be functionally mosaic for GPI-AP expression. Granulocytes from the mother of patients 3 and 4 showed a significantly decreased expression of CD16 (figure e-2, upper panels), whereas those from the mother of patient 5 showed normal expression (figure e-2, lower panels). The mothers appeared to have no neurologic disorder, suggesting that GPI-sufficient cells may preferentially proliferate in the brain during early embryogenesis.

Functional analysis. *PIGA* cDNAs bearing patient mutations were functionally analyzed by transfecting them into *PIGA*-deficient B lymphoblastoid cells (JY5) and measuring the surface expression of GPI-APs.

© 2014 American Academy of Neurology. Unauthorized reproduction of this article is prohibited.

Figure 3 Flow cytometry of granulocytes

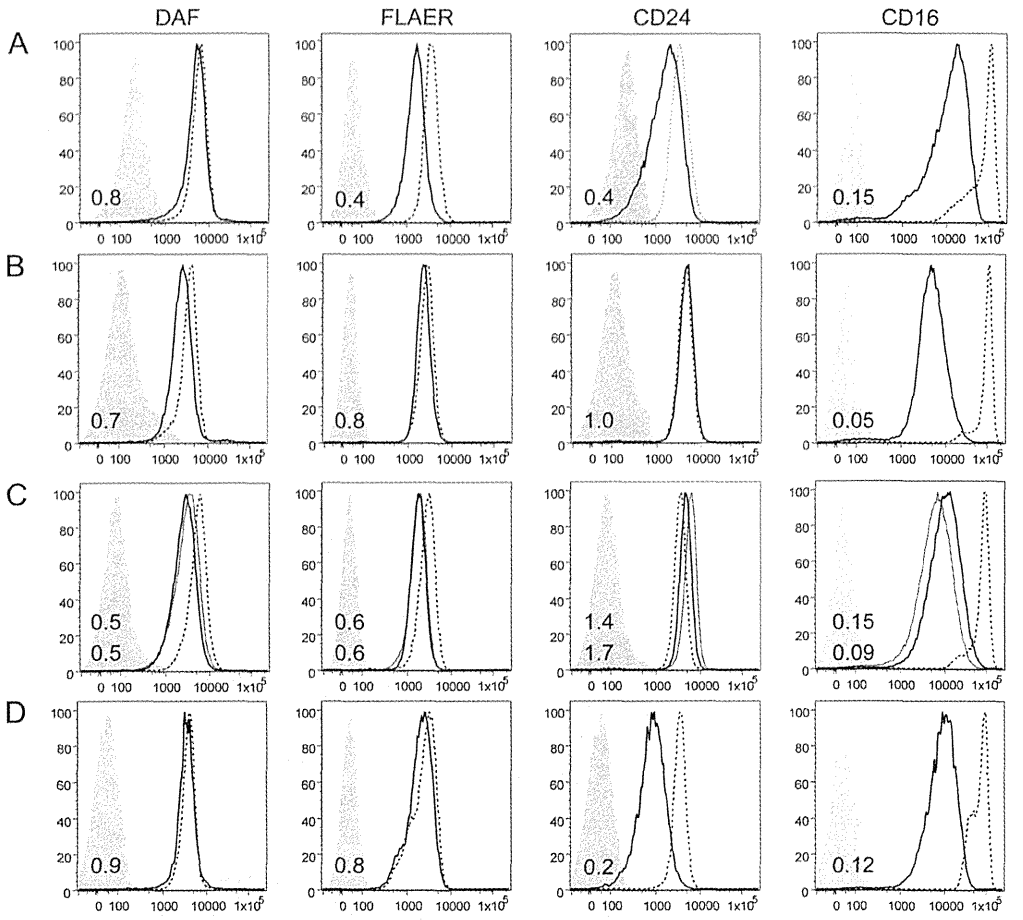

Flow cytometry of patient 1 (R412X) (A), patient 2 (I206F) (B), patients 3 and 4 (2 brothers, R77L) (C), and patient 5 (R119W) (D). In all families, the surface expression of various glycosylphosphatidylinositol-anchored proteins on patient granulocytes (solid lines; patients 3 and 4 are shown in C as thin and thick lines, respectively) was severely decreased compared with the normal control (dotted lines). Light shadows represent isotype controls. Mean fluorescent intensities of each sample against a normal control are shown in each panel (upper, patient 4; lower, patient 3 in C).

When strong promoter (SRα)-driven constructs were used, R412X mutant cDNA completely restored the surface expression of CD59, DAF, and CD48, whereas R412 truncated cDNA had no activity (figure 4A), suggesting that a small amount of full-length PIGA protein was generated by readthrough of a stop codon. When weak promoter-driven constructs (pTA) were used instead, R412X cDNA could not restore the surface expression of GPI-APs, whereas it was completely restored by wild-type cDNA (figure 4B). Similarly, the strong promoter (SRα)-driven I206F and R77L mutant PIGAs completely restored the surface expression of GPI-APs, whereas the weak promoter-driven mutant constructs only partially restored this (figure 4, C–F). Levels of expressed mutant PIGA proteins were similar to or even higher than wild-type levels (figure e-3). A faint band representing full-length PIGA protein harboring R412X could be detected (figure e-3, lane 4), which was consistent with the functional analysis. From these results, we concluded that these mutations affect the PIGA activity leading to inherited GPI deficiency.

DISCUSSION We have identified 4 *PIGA* mutations in 172 probands from a variety of EOEE-affected families, such as EME (n = 1), West syndrome (n = 2), and unclassified EOEE in a sibling. Myoclonus and suppression burst on EEG were recognized in 2 patients with West syndrome and the patient with EME in our cohort, as well as the previously reported family.[11] Indeed, myoclonus and suppression burst on EEG appear to be characteristic features for patients with a *PIGA* mutation.

Other clinical features such as polyhydramnios, facial dysmorphism, joint contractures, hypotonia, and severe developmental delay are recurrently seen in patients with *PIGA* mutations. A previous report of 3 patients with the same nonsense mutation,

© 2014 American Academy of Neurology. Unauthorized reproduction of this article is prohibited.

Figure 4 Functional analysis of the mutant PIGA

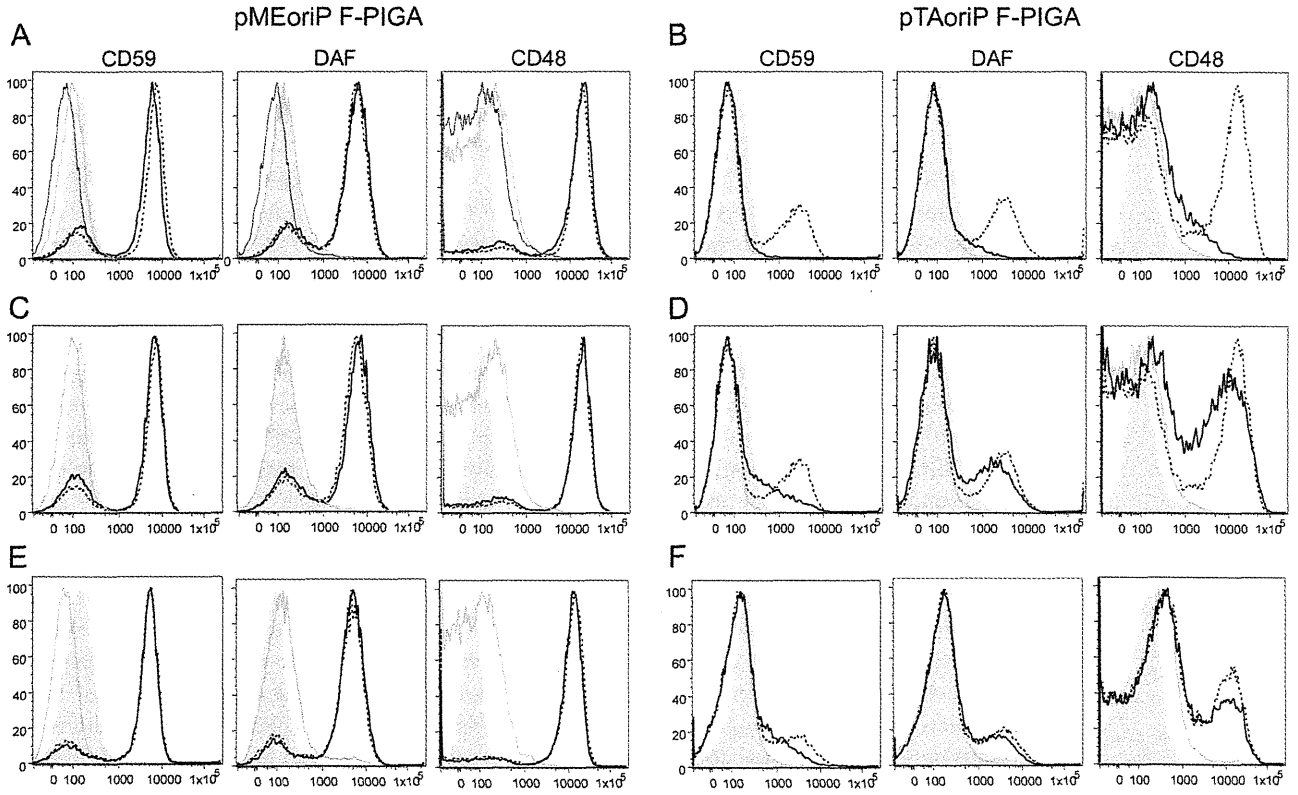

JY5 cells were transiently transfected with pMEoriP (strong SRα promoter-driven, Epstein-Barr [EB] virus origin-containing vector) (panels A, C, and E) or pTAoriP F-PIGA (weak TATA box promoter-driven, EB virus origin-containing vector) (panels B, D, and F) bearing various FLAG-tagged PIGA complementary DNAs. Restoration of the surface expression of CD59, DAF, and CD48 was assessed 2 days later by flow cytometry. Dotted lines represent wild-type PIGA, thick lines represent mutant PIGA, thin lines represent truncated PIGA, and shadows represent isotype controls. (A) Strong promoter-driven R412X PIGA (thick lines) completely rescued the expression of glycosylphosphatidylinositol-anchored proteins (GPI-APs) similar to wild-type PIGA (dotted lines), whereas R412-truncated PIGA (thin lines) had no activity. (B) Weak promoter-driven R412X PIGA (thick lines) did not rescue the surface expression of GPI-APs, whereas wild-type PIGA (dotted lines) did. (C) Strong promoter-driven I206F PIGA (thick lines) completely rescued the expression of GPI-APs similar to wild-type PIGA (dotted lines). (D) Weak promoter-driven I206F PIGA (thick lines) did not rescue the surface expression of GPI-APs, whereas wild-type PIGA (dotted lines) did. (E) Strong promoter-driven R77L PIGA (thick lines) completely rescued the expression of GPI-APs similar to wild-type PIGA (dotted lines). (F) Weak promoter-driven R77L PIGA (thick lines) did not rescue the surface expression of CD59, whereas wild-type PIGA (dotted lines) did.

R412X,[11] as patient 1 in our cohort showed similar or more severe clinical features, such as a large occipitofrontal circumference at birth, early-onset intractable seizures, and severe respiratory failure leading to early death or mechanical ventilation. Complete disruption of the *PIGA* gene results in early embryonic lethality in male mice, while heterozygous female mice have late embryonic lethality, insufficient closure of the neural tube, and a cleft palate.[21] In the present study, a reduced but definite expression of GPI-APs in the granulocytes of patients with R412X and a complete restoration of GPI-AP surface expression by the transfection of R412X mutant cDNA under the control of a strong promoter suggest that small amounts of full-length PIGA protein were generated by the read-through of a stop codon because the cDNA truncated at R412 showed no activity.

The siblings with the *PIGA* p.R77L mutation demonstrated milder clinical symptoms compared with patients with other *PIGA* mutations. They showed neither dysmorphisms nor severe motor disturbance, the onset of their seizures was relatively late, and the findings of their initial EEG and brain MRI were normal. Flow cytometry only revealed a decreased expression of CD16, which contrasts with the more severe phenotype of patient 1 and associated decreased levels of CD16, FLAER, and CD24. According to the functional study using *PIGA*-deficient B lymphoblasts transfected with a weak promoter-driven mutant *PIGA*, the activity of the R77L mutant was higher than that of other mutants. Thus, the phenotype severity appears to correlate with genotype and the residual functional activity of the PIGA protein.

Patients 2 and 5 showed peculiarly high signals on DWI at the specific areas of the brainstem, basal ganglia, thalamus, and deep white matter, particularly the optic radiation as previously reported in patient 1.[22] Although delayed myelination and the volume loss of

© 2014 American Academy of Neurology. Unauthorized reproduction of this article is prohibited.

white matter including a thin corpus callosum, mild brain atrophy, and mild cerebellar hypoplasia are frequently seen in patients with mutations in other genes involved in the biosynthesis of the GPI anchor, such as *PIGN*, *PGAP2*, *DPM1*, and *DPM2*,[10,15,23,24] high signals on DWI have never been reported. In addition, the ADC map showed adversely low or decreased signals, suggesting restricted water diffusion. This pattern (a high DWI signal and low ADC values) can be seen in patients with specific metabolic disorders, such as nonketotic hyperglycinemia, phenylketonuria, maple syrup urine disease, Leigh encephalopathy, infantile neuroaxonal dystrophy, Wilson disease, metachromatic leukodystrophy, and Canavan disease.[25] Indeed, metabolic disorders, particularly nonketotic hyperglycinemia, are strongly associated with EME, which is common in patients with *PIGA* mutations. A brain MRI of a patient in early infancy with a recently reported *PIGO* deficiency also showed hypomyelination and abnormally high signals in T2-weighted images from the bilateral basal ganglia to the brainstem.[26] While the pathologic mechanism for restricted diffusion patterns in specific areas is unknown, this finding may be useful to screen patients with a GPI deficiency.

Patients with the severe type of *PIGA* mutation showed both an asymmetrical and symmetrical pattern of suppression burst on EEG in this study. The suppression burst pattern is characteristic for 2 types of EOEE, OS and EME, and most patients of both disorders show a symmetrical pattern. The asymmetrical pattern has been reported in patients with agenesis of the corpus callosum such as Aicardi syndrome,[27] and *KCNQ2* mutations.[4] All 3 patients with the asymmetrical suppression burst in the present study also showed white matter immaturity with a thin corpus callosum and abnormally high signals in deep white matter on DWI. These data indicate a disturbed connectivity of the bilateral hemisphere in patients with *PIGA* mutations. The adverse advancement of the EEG findings from hypsarrhythmia to suppression burst in our cases, which is usually observed in neonates, might reflect the retrogression of brain function, which is also seen in the progression of brain atrophy.

Patient 1 showed severe hydronephrosis caused by the vesicoureteral reflux and hepatoblastoma, so a diagnosis of Schinzel-Giedion syndrome was made. This is an autosomal dominant disorder characterized by severe developmental delay, distinctive facial features with a prominent forehead, midface retraction, short, upturned nose, and either hydronephrosis or typical skeletal malformations, such as sclerotic skull base, wide occipital synchondrosis, increased cortical density or thickness, and broad ribs.[28] *SETBP1* mutations have been reported in patients with Schinzel-Giedion syndrome[29] but were not identified in our patient. Because of the phenotypic similarities between patients with *PIGA* mutation and those with Schinzel-Giedion syndrome, we suggest that patients with Schinzel-Giedion syndrome with no *SETBP1* mutations should undergo genetic analysis of their *PIGA* gene or other genes involved in the biosynthesis of the GPI anchor.

Patients with mutations in *PIGL*, *PIGM*, *PIGN*, *PIGO*, *PIGT*, *DPM2*, and *MPDU1* often die in early childhood.[9,12,14–16,23,30] While pneumonia is the main cause of death in these patients, intractable seizures, which rigorously worsen the prognosis of life expectancy and cognitive function, frequently occur. It is of interest that the targeted agents butyrate and pyridoxine were reported to be effective for seizure treatment in patients with *PIGM* or *PIGO* mutation, respectively.[26,31] However, patient 5 in this study did not respond to pyridoxine. The study of more patients will facilitate the establishment of personalized treatment methods for patients with GPI deficiencies.

Our study demonstrated that mutations in *PIGA* are causative for a variety of EOEEs, particularly for patients with myoclonus and asymmetrical suppression burst on EEG. Multiple anomalies with facial dysmorphism resembling Schinzel-Giedion syndrome, delayed myelination with restricted diffusion patterns at the brainstem, and deep white matter are key findings in a severe form in patients with *PIGA* mutations. Nevertheless, a wide range of clinical phenotypes of *PIGA* mutations should be kept in mind, including the less severe forms involving intellectual disability and treatable seizures without facial dysmorphism.

AUTHOR CONTRIBUTIONS

Mitsuhiro Kato: study concept and design, analysis of the clinical data, interpretation of the data, and drafting/revising of the manuscript. Hirotomo Saitsu: study concept and design, analysis of the genetic data, interpretation of the data, and drafting/revising of the manuscript. Yoshiko Murakami: study concept and design, analysis of the biological data, interpretation of the data, and drafting/revising of the manuscript. Kenjiro Kikuchi, Shuei Watanabe, Mizue Iai, Kazushi Miya, Ryuki Matsuura, and Rumiko Takayama: analysis of the clinical data and sample collection. Chihiro Ohba, Mitsuko Nakashima, Yoshinori Tsurusaki, and Noriko Miyake: analysis of the genetic data. Shin-ichiro Hamano and Hitoshi Osaka: analysis of the clinical data and sample collection. Kiyoshi Hayasaka: analysis of the clinical data and revising of the manuscript. Taroh Kinoshita: analysis of the biological data, interpretation of the data, and drafting/revising of the manuscript. Naomichi Matsumoto: study concept and design, analysis of the genetic data, interpretation of the data, and drafting/revising of the manuscript.

ACKNOWLEDGMENT

The authors are grateful to the patients and their families for their participation in this study. The authors thank Keiko Tanaka, Kana Miyanagi, Nobuko Watanabe, and Kiyomi Masuko for their technical assistance.

STUDY FUNDING

This study was supported by the Ministry of Health, Labour and Welfare of Japan (25140101, 24133701,11103577, 11103340, 10103235), a Grant-in-Aid for Scientific Research (A), (B), and (C) from the Japan

© 2014 American Academy of Neurology. Unauthorized reproduction of this article is prohibited.

Society for the Promotion of Science (A: 24249019, B: 25293085 25293235, C: 24591500, 23590363), the Takeda Science Foundation, the fund for Creation of Innovation Centers for Advanced Interdisciplinary Research Areas Program in the Project for Developing Innovation Systems, the Strategic Research Program for Brain Sciences (11105137), and a Grant-in-Aid for Scientific Research on Innovative Areas (transcription cycle, exploring molecular basis for brain diseases based on personal genomics) from the Ministry of Education, Culture, Sports, Science and Technology of Japan (12024421, 25129705).

DISCLOSURE

M. Kato is funded by research grants from the Ministry of Health, Labour and Welfare of Japan, and a Grant-in-Aid for Scientific Research (C) from the Japan Society for the Promotion of Science. H. Saitsu is funded by a Grant-in-Aid for Scientific Research (B) from the Japan Society for the Promotion of Science, and the Takeda Science Foundation. Y. Murakami is funded by a Grant-in-Aid for Scientific Research (C) from the Japan Society for the Promotion of Science, the Takeda Science Foundation, a Grant-in-Aid for Scientific Research on Innovative Areas (exploring molecular basis for brain diseases based on personal genomics) from the Ministry of Education, Culture, Sports, Science and Technology of Japan. K. Kikuchi, S. Watanabe, M. Iai, K. Miya, R. Matsuura, R. Takayama, C. Ohba, M. Nakashima, and Y. Tsurusaki report no disclosures relevant to the manuscript. N. Miyake is funded by research grants from the Ministry of Health, Labour and Welfare of Japan, a Grant-in-Aid for Scientific Research (B) from the Japan Society for the Promotion of Science, and the Takeda Science Foundation. S. Hamano, H. Osaka, and K. Hayasaka report no disclosures relevant to the manuscript. T. Kinoshita is supported by a Grant-in-Aid for Scientific Research (A) from the Japan Society for the Promotion of Science. N. Matsumoto is supported by grants from the Ministry of Health, Labour and Welfare of Japan, a Grant-in-Aid for Scientific Research (A) from the Japan Society for the Promotion of Science, the Takeda Science Foundation, the fund for Creation of Innovation Centers for Advanced Interdisciplinary Research Areas Program in the Project for Developing Innovation Systems, the Strategic Research Program for Brain Sciences, a Grant-in-Aid for Scientific Research on Innovative Areas (transcription cycle) from the Ministry of Education, Culture, Sports, Science and Technology of Japan. Go to Neurology.org for full disclosures.

Received November 7, 2013. Accepted in final form February 7, 2014.

REFERENCES

1. Kato M, Saitoh S, Kamei A, et al. A longer polyalanine expansion mutation in the *ARX* gene causes early infantile epileptic encephalopathy with suppression-burst pattern (Ohtahara syndrome). Am J Hum Genet 2007;81:361–366.
2. Saitsu H, Kato M, Mizuguchi T, et al. De novo mutations in the gene encoding STXBP1 (MUNC18-1) cause early infantile epileptic encephalopathy. Nat Genet 2008;40: 782–788.
3. Saitsu H, Kato M, Osaka H, et al. *CASK* aberrations in male patients with Ohtahara syndrome and cerebellar hypoplasia. Epilepsia 2012;53:1441–1449.
4. Kato M, Yamagata T, Kubota M, et al. Clinical spectrum of early onset epileptic encephalopathies caused by *KCNQ2* mutation. Epilepsia 2013;54:1282–1287.
5. Nakamura K, Kato M, Osaka H, et al. Clinical spectrum of *SCN2A* mutations expanding to Ohtahara syndrome. Neurology 2013;81:992–998.
6. Kato M. A new paradigm for West syndrome based on molecular and cell biology. Epilepsy Res 2006;70(suppl 1): S87–S95.
7. Saitsu H, Tohyama J, Kumada T, et al. Dominant-negative mutations in alpha-II spectrin cause West syndrome with severe cerebral hypomyelination, spastic quadriplegia, and developmental delay. Am J Hum Genet 2010;86:881–891.
8. Kurian MA, Meyer E, Vassallo G, et al. Phospholipase C beta 1 deficiency is associated with early-onset epileptic encephalopathy. Brain 2010;133:2964–2970.
9. Almeida AM, Murakami Y, Layton DM, et al. Hypomorphic promoter mutation in *PIGM* causes inherited glycosylphosphatidylinositol deficiency. Nat Med 2006;12: 846–851.
10. Hansen L, Tawamie H, Murakami Y, et al. Hypomorphic mutations in *PGAP2*, encoding a GPI-anchor-remodeling protein, cause autosomal-recessive intellectual disability. Am J Hum Genet 2013;92:575–583.
11. Johnston JJ, Gropman AL, Sapp JC, et al. The phenotype of a germline mutation in *PIGA*: the gene somatically mutated in paroxysmal nocturnal hemoglobinuria. Am J Hum Genet 2012;90:295–300.
12. Krawitz PM, Murakami Y, Hecht J, et al. Mutations in *PIGO*, a member of the GPI-anchor-synthesis pathway, cause hyperphosphatasia with mental retardation. Am J Hum Genet 2012;91:146–151.
13. Krawitz PM, Schweiger MR, Rodelsperger C, et al. Identity-by-descent filtering of exome sequence data identifies *PIGV* mutations in hyperphosphatasia mental retardation syndrome. Nat Genet 2010;42:827–829.
14. Kvarnung M, Nilsson D, Lindstrand A, et al. A novel intellectual disability syndrome caused by GPI anchor deficiency due to homozygous mutations in *PIGT*. J Med Genet 2013;50:521–528.
15. Maydan G, Noyman I, Har-Zahav A, et al. Multiple congenital anomalies-hypotonia-seizures syndrome is caused by a mutation in *PIGN*. J Med Genet 2011;48: 383–389.
16. Ng BG, Hackmann K, Jones MA, et al. Mutations in the glycosylphosphatidylinositol gene *PIGL* cause CHIME syndrome. Am J Hum Genet 2012;90:685–688.
17. DePristo MA, Banks E, Poplin R, et al. A framework for variation discovery and genotyping using next-generation DNA sequencing data. Nat Genet 2011; 43:491–498.
18. Saitsu H, Nishimura T, Muramatsu K, et al. De novo mutations in the autophagy gene *WDR45* cause static encephalopathy of childhood with neurodegeneration in adulthood. Nat Genet 2013;45:445–449.
19. Wang K, Li M, Hakonarson H. ANNOVAR: functional annotation of genetic variants from high-throughput sequencing data. Nucleic Acids Res 2010;38:e164.
20. Molinari F, Raas-Rothschild A, Rio M, et al. Impaired mitochondrial glutamate transport in autosomal recessive neonatal myoclonic epilepsy. Am J Hum Genet 2005;76: 334–339.
21. Nozaki M, Ohishi K, Yamada N, Kinoshita T, Nagy A, Takeda J. Developmental abnormalities of glycosylphosphatidylinositol-anchor-deficient embryos revealed by Cre/loxP system. Lab Invest 1999;79:293–299.
22. Watanabe S, Murayama A, Haginoya K, et al. Schinzel-Giedion syndrome: a further cause of early myoclonic encephalopathy and vacuolating myelinopathy. Brain Dev 2012;34:151–155.
23. Barone R, Aiello C, Race V, et al. DPM2-CDG: a muscular dystrophy-dystroglycanopathy syndrome with severe epilepsy. Ann Neurol 2012;72:550–558.
24. Yang AC, Ng BG, Moore SA, et al. Congenital disorder of glycosylation due to *DPM1* mutations presenting with dystroglycanopathy-type congenital muscular dystrophy. Mol Genet Metab 2013;110:345–351.

© 2014 American Academy of Neurology. Unauthorized reproduction of this article is prohibited.

25. Sener RN. Diffusion magnetic resonance imaging patterns in metabolic and toxic brain disorders. Acta Radiol 2004; 45:561–570.
26. Kuki I, Takahashi Y, Okazaki S, et al. Vitamin B6-responsive epilepsy due to inherited GPI deficiency. Neurology 2013; 81:1467–1469.
27. Aicardi J. Aicardi syndrome. Brain Dev 2005;27: 164–171.
28. Lehman AM, McFadden D, Pugash D, Sangha K, Gibson WT, Patel MS. Schinzel-Giedion syndrome: report of splenopancreatic fusion and proposed diagnostic criteria. Am J Med Genet A 2008;146A: 1299–1306.
29. Hoischen A, van Bon BW, Gilissen C, et al. De novo mutations of *SETBP1* cause Schinzel-Giedion syndrome. Nat Genet 2010;42:483–485.
30. Kranz C, Denecke J, Lehrman MA, et al. A mutation in the human *MPDU1* gene causes congenital disorder of glycosylation type If (CDG-If). J Clin Invest 2001;108:1613–1619.
31. Almeida AM, Murakami Y, Baker A, et al. Targeted therapy for inherited GPI deficiency. N Engl J Med 2007;356: 1641–1647.

Enjoy Big Savings on NEW 2014 AAN Practice Management Webinars Subscriptions

The American Academy of Neurology offers 14 cost-effective Practice Management Webinars you can attend live or listen to recordings posted online. AAN members can purchase one webinar for $149 or subscribe to the entire series for only $199. *This is new pricing for 2014 and significantly less than 2013*—and big savings from the new 2014 nonmember price of $199 per webinar or $649 for the subscription. Register today for these and other 2014 webinars at *AAN.com/view/pmw14*:

April 8 – How PQRS Quality Measures Will Inform Future Medicare Value-based Payments

May 13 – Measuring and Improving Your Patients' Experience

June 18 – Using Practice Benchmarking Analytics to Improve Your Bottom Line

Visit the *Neurology*® Web Site at www.neurology.org

- Enhanced navigation format
- Increased search capability
- Highlighted articles
- Detailed podcast descriptions
- RSS Feeds of current issue and podcasts
- Personal folders for articles and searches
- Mobile device download link
- AAN Web page links
- Links to Neurology Now®, Neurology Today®, and Continuum®
- Resident & Fellow subsite

Find *Neurology*® on Facebook: http://tinyurl.com/neurologyfan

Follow *Neurology*® on Twitter: https://twitter.com/GreenJournal

© 2014 American Academy of Neurology. Unauthorized reproduction of this article is prohibited.

CLINICAL GENETICS An International Journal of Genetics, Molecular and Personalized Medicine

Clin Genet 2014: 85: 396–398
Printed in Singapore. All rights reserved

© 2013 John Wiley & Sons A/S.
Published by John Wiley & Sons Ltd
CLINICAL GENETICS
doi: 10.1111/cge.12188

Letter to the Editor

AKT3 and *PIK3R2* mutations in two patients with megalencephaly-related syndromes: MCAP and MPPH

To the Editor:

Megalencephaly-capillary malformation syndrome (MCAP) and megalencephaly-polymicrogyria-polyd actyly-hydrocephalus syndrome (MPPH) belong to a spectrum of megalencephaly-related syndromes. The diagnostic criteria for MCAP include megalencephaly plus capillary malformations or syndactyly, and those for MPPH include megalencephaly and polymicrogyria, an absence of vascular anomalies, syndactyly, and brain heterotopia (1). Recently, *AKT3*, *PIK3R2*, and *PIK3CA* mutations have been identified in MCAP and MPPH (2). The proteins encoded by these genes are core components of the phosphatidylinositol 3-kinase (PI3K)-AKT pathway (3). Here, we report two patients with an *AKT3* and *PIK3R2* mutation. The study protocol was approved by the Institutional Review Boards for Ethical Issues at Yokohama City University and Yamagata University.

Patient 1 is an 8-year-old girl who has been previously reported as having MPPH (4). Brain magnetic resonance imaging (MRI) at 6 years showed asymmetry of the gyral pattern, dilated lateral ventricles, polymicrogyria, and abnormal signals in the occipital lobes, suggesting dysmyelination (Fig. 1a–c). Patient 2 is a 2-month-old boy who showed macrocephaly, cutis marmorata of the distal extremities, and hyperextensibility

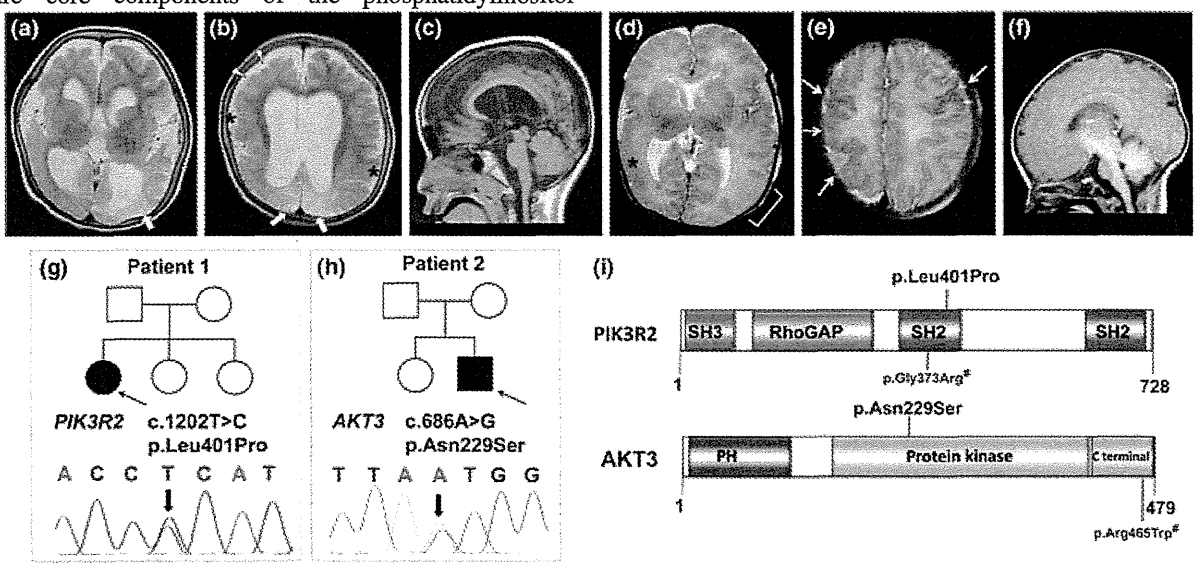

Fig. 1. Magnetic resonance imaging of patient 1 at 6 years of age (**a–c**). (**a**, **b**) Axial T2-weighted imaging showing enlarged lateral and third ventricles, enlarged extra-axial space, and decreased white matter volume with occipital lobe predominance. Irregular small gyri with areas of cortical thickening compatible with polymicrogyria are observed prominently in the bilateral perisylvian regions (asterisks) and the right frontal lobes (white arrowheads). Abnormal high-intensity signals are seen in the bilateral occipital lobes (thick white arrows). (c) Sagittal T1-weighted imaging showing normal brainstem and cerebellum. Magnetic resonance imaging of patient 2 at 7 days of age (**d–f**). (**d**) Axial T2-weighted imaging at the level of the basal ganglia showing enlargement of the left hemisphere. Polymicrogyria is seen in the perisylvian fissures with right-side dominance, which extends to the right temporal lobe (asterisk). The left parietal cortex shows a blurred border between the gray matter and the white matter (bracket), suggesting dysplasia of cortical development. (**e**) Axial T2-weighted imaging showing polymicrogyria in the right parietal lobe adjacent to the central sulcus (white arrows). (**f**) Sagittal T1-weighted imaging showing a relatively small pontine base. Family pedigrees and causative mutations (**g–i**). (**g**) Patient 1 with MPPH showing a *de novo* heterozygous missense mutation in *PIK3R2* (c.1202T>C, p.Leu401Pro). (h) Patient 2 with MCAP showing a *de novo* missense heterozygous mutation in *AKT3* (c.686A>G, p.Asn229Ser). (i) Distribution of mutations in *PIK3R2* and *AKT3*. SH2, Src homology 2 domain; SH3, Src homology 3 domain; RhoGAP, Rho GTPase-activating protein domain; PH, pleckstrin homology domain. #Reported by Riviere et al. (2).

of the skin. Brain MRI at 7 days showed an asymmetric cerebral hemisphere with right-dominant perisylvian polymicrogyria (Fig. 1d–f), and at 2 months showed a thin corpus callosum and progressive hydrocephalus. These findings were compatible with MCAP.

Whole exome sequencing using DNA extracted from blood leukocytes revealed a *de novo* missense mutation in each patient: p.Leu401Pro in *PIK3R2* (patient 1) and p.Asn229Ser in *AKT3* (patient 2) (Fig. 1g–i). Both mutations were absent from the 6500 eomes sequenced by the National Heart, Lung, and Blood Institute exome project and our 144 in-house control exomes. The read count for mutant alleles possessing p.Leu401Pro in *PIK3R2* was 47.7% (84/176 reads), and that for p.Asn229Ser in *AKT3* was 52.2% (128/245 reads). Therefore, these mutations are likely germline rather than mosaic mutations.

The novel *PIK3R2* mutation (p.Leu401Pro) in patient 1 is within the first Src homology 2 (SH2) domain of the PIK3R2 protein; this domain binds to phosphotyrosine-containing motifs and regulates many aspects of cellular communication (5). Eleven MPPH families have been reported to have a recurrent *PIK3R2* mutation (p.Gly373Arg), which is also located in the first SH2 domain (2). The phenotypes of all 13 cases with the p.Gly373Arg mutation were similar to that of patient 1 (Table 1) (1, 2), implying that impaired function of the SH2 domain is important in the pathogenesis of MPPH. The *AKT3* mutation (p.Asn229Ser) detected in patient 2 with MCAP has been reported in a case of MPPH (2). Furthermore, another case with a different *AKT3* mutation (p.Arg465Trp) was diagnosed with overlapping features of MCAP and MPPH (Table 1). These findings support the notion that the two syndromes have a common genetic basis. Interestingly, somatic mosaicism of an *AKT3* mutation causes hemimegalencephaly, which is similar to MPPH or MCAP (6, 7). Mutation screening of *AKT3* should be considered for patients with MPPH or MCAP as well as those with hemimegalencephaly, for whom pathological tissue is available.

MCAP and MPPH are categorized as overgrowth syndromes, as are Cowden disease and Proteus syndrome that are caused by abnormal activation of the PI3K–AKT pathway, which participates in diverse cellular processes (3, 8). The PI3K–AKT pathway is linked to mammalian target of rapamycin (mTOR) (6), which is a specific molecule for targeted therapeutics (sirolimus or everolimus). Further investigation into potential treatments for overgrowth syndromes is essential.

In summary, we have described two patients with either an *AKT3* or a *PIK3R2* mutation. Our data highlight the importance of the SH2 domain of PIK3R2 in MPPH, and support that MPPH and MCAP have the same genetic origin.

Acknowledgements

We would like to thank the patients and their families for their participation in this study. We thank Aya Narita for technical

Table 1. Phenotypes associated with *PIK3R2* and *AKT3* mutations

Patient (diagnosis)	Patient 1 (MPPH)	13 patients[a] (MPPH)	Patient 2 (MCAP)	LR11-354[a] (MPPH)	LR08-018[a] (overlapping MCAP and MPPH)
Mutation	*PIK3R2* (p.Leu401Pro)	*PIK3R2* (p.Gly373Arg)	*AKT3* (p.Asn229Ser)	*AKT3* (p.Asn229Ser)	*AKT3* (p.Arg465Trp)
Features					
HC SD (age)	+2.6 (1 y 9 m)	+2–8 (8 m–13 y)	+3.0 (2 m)	+6.0 (2 y 5 m)	+5.5 (7.5 m)
Overgrowth	–	2/13	–	–	–
Vascular abnormalities	–	0/13	Skin capillary malformation	–	umbilical hemangioma
Connective tissue dysplasia	–	0/13	+	+	+
Syndactyly	–	0/13	–	–	–
Polydactyly	+	2/13	–	–	–
Epileptic seizures	+	6/9	+	ND	+
Visual impairment	+	ND	–	ND	ND
Neuroimaging features					
Polymicrogyria	+	13/13	+	+	+
Hydrocephalus or ventriculomegaly	+	13/13	+	+	+
CBTE	–	8/13	–	–	+

MPPH, megalencephaly-polymicrogyria-polydactyly-hydrocephalus syndrome; MCAP, megalencephaly-capillary malformation syndrome; HC, head circumference; SD, standard deviation; y, years; m, months; ND, no data; CBTE, cerebellar tonsillar ectopia.

[a] Riviere et al. (2) and Mirzaa et al. (1).

assistance. This work was supported by the Ministry of Health, Labour, and Welfare of Japan (24133701,11103577, 11103340 and 10103235); a Grant-in-Aid for Scientific Research (C) from the Japan Society for the Promotion of Science (24591500); a Grant-in-Aid for Young Scientists from the Japan Society for the Promotion of Science (10013428 and 12020465); the Takeda Science Foundation; the Japan Science and Technology Agency; the Strategic Research Program for Brain Sciences (11105137); and a Grant-in-Aid for Scientific Research on Innovative Areas (Transcription Cycle) from the Ministry of Education, Culture, Sports, Science, and Technology of Japan (12024421).

K. Nakamura[a,b]
M. Kato[b]
J. Tohyama[c]
T. Shiohama[d]
K. Hayasaka[b]
K. Nishiyama[a]
H. Kodera[a]
M. Nakashima[a]
Y. Tsurusaki[a]
N. Miyake[a]
N. Matsumoto[a]
H. Saitsu[a]
[a]Department of Human Genetics
Yokohama City University Graduate School of Medicine
Yokohama, Japan
[b]Department of Pediatrics
Yamagata University Faculty of Medicine
Yamagata, Japan
[c]Department of Pediatrics
Epilepsy Center, Nishi-Niigata Chuo National Hospital
Niigata, Japan
[d]Department of Pediatrics
Kimitsu Chuo Hospital
Chiba, Japan

References

1. Mirzaa GM, Conway RL, Gripp KW et al. Megalencephaly-capillary malformation (MCAP) and megalencephaly-polydactyly-poly microgyria-hydrocephalus (MPPH) syndromes: two closely related disorders of brain overgrowth and abnormal brain and body morphogenesis. Am J Med Genet A 2012: 158A: 269–291.
2. Riviere JB, Mirzaa GM, O'Roak BJ et al. De novo germline and postzygotic mutations in *AKT3*, *PIK3R2* and *PIK3CA* cause a spectrum of related megalencephaly syndromes. Nat Genet 2012: 44: 934–940.
3. Franke TF. PI3K/Akt: getting it right matters. Oncogene 2008: 27: 6473–6488.
4. Tohyama J, Akasaka N, Saito N, Yoshimura J, Nishiyama K, Kato M. Megalencephaly and polymicrogyria with polydactyly syndrome. Pediatr Neurol 2007: 37: 148–151.
5. Liu BA, Jablonowski K, Raina M, Arcé M, Pawson T, Nash PD. The human and mouse complement of SH2 domain proteins – establishing the boundaries of phosphotyrosine signaling. Mol Cell 2006: 22: 851–868.
6. Lee JH, Huynh M, Silhavy JL et al. De novo somatic mutations in components of the PI3K-AKT3-mTOR pathway cause hemimegalencephaly. Nat Genet 2012: 44: 941–945.
7. Poduri A, Evrony GD, Cai X et al. Somatic activation of AKT3 causes hemispheric developmental brain malformations. Neuron 2012: 74: 41–48.
8. Lindhurst MJ, Sapp JC, Teer JK et al. A mosaic activating mutation in *AKT1* associated with the Proteus syndrome. N Engl J Med 2011: 365: 611–619.

Correspondence:
Dr Kazuyuki Nakamura, MD
Department of Pediatrics
Yamagata University Faculty of Medicine
2-2-2 Iida-nishi
Yamagata 990-9585
Japan
Tel: +81-23-628-5329
Fax: +81-23-628-5331
e-mail: kazun-yamagata@umin.ac.jp

Ehlers–Danlos Syndrome Associated with Glycosaminoglycan Abnormalities

10

Noriko Miyake, Tomoki Kosho, and Naomichi Matsumoto

Abstract

Ehlers–Danlos syndrome (EDS) is a genetically and clinically heterogeneous group of connective tissue disorders that typically present with skin hyperextensibility, joint hypermobility, and tissue fragility. The major cause of EDS appears to be impaired biosynthesis and enzymatic modification of collagen. In this chapter, we discuss two types of EDS that are associated with proteoglycan abnormalities: the progeroid type of EDS and dermatan 4-*O*-sulfotransferase 1 (D4ST1)-deficient EDS. The progeroid type of EDS is caused by mutations in *B4GALT7* or *B3GALT6*, both of which encode key enzymes that initiate glycosaminoglycan (GAG) synthesis. D4ST1-deficient EDS is caused by mutations in *CHST14*, which encodes an enzyme responsible for post-translational modification of GAG. The clinical and molecular characteristics of both types of EDS are described in this chapter.

Keywords

Ehlers–Danlos syndrome (EDS) • Progeroid type • *B4GALT7* • *B3GALT6* • Xylosylprotein beta 1,4-galactosyltransferase, polypeptide 7 • UDP-Gal:βGal β 1,3-galactosyltransferase polypeptide 6 • Dermatan 4-*O*-sulfotransferase 1 (D4ST1)-deficient EDS • *CHST14*

N. Miyake (✉) • N. Matsumoto
Department of Human Genetics, Yokohama City University Graduate School of Medicine, 3-9 Fukuura, Kanazawa-ku, Yokohama, 236-0004, Japan
e-mail: nmiyake@yokohama-cu.ac.jp; naomat@yokohama-cu.ac.jp

T. Kosho
Department of Medical Genetics, Shinshu University School of Medicine, 3-1-1 Asahi, Matsumoto, 390-8621, Japan
e-mail: ktomoki@shinshu-u.ac.jp

J. Halper (ed.), *Progress in Heritable Soft Connective Tissue Diseases*, Advances in Experimental Medicine and Biology 802, DOI 10.1007/978-94-007-7893-1_10, © Springer Science+Business Media Dordrecht 2014

Abbreviations

CHST14	Carbohydrate (*N*-Acetylgalactosamine 4-*O*) Sulfotransferase 14
D4ST1	Dermatan 4-*O*-sulfotransferase 1
EDS	Ehlers–Danlos Syndrome
GAG	Glycosaminoglycan
Gal	Galactose
GalNAc	*N*-Acetylgalactosamine
GlcA	Glucuronic Acid
IdoA	Iduronic Acid
PG	Proteoglycan
Xyl	Xylose

10.1 Introduction

Ehlers–Danlos syndrome (EDS) is a heterogeneous connective tissue disorder that affects as many as 1 in 5,000 individuals. It is characterized by joint and skin laxity, and tissue fragility [44]. In a revised classification, Beighton et al. classified EDS into six major types and several minor types [2]. The major causes of EDS are thought to include abnormal collagen biosynthesis through dominant-negative effects, haploinsufficiency of mutant procollagen α-chains, or deficiencies in collagen processing enzymes [29]. Abnormal glycosaminoglycan (GAG) synthesis and incorrect post-translational modification of GAG in proteoglycans (PGs) were recently identified in the progeroid type of EDS (EDS, progeroid form; MIM#130070, MIM#615349) and dermatan 4-*O*-sulfotransferase 1 (D4ST1)-deficient EDS (EDS, musculocontractural type; MIM#601776), respectively. In this chapter, the clinical and molecular characteristics of both types of EDS are described.

10.2 Background

Glycosylation is the addition of a sugar chain (a glycan) to a protein (generating a glycoprotein) or lipid (generating a glycolipid). More than 40 human disorders are thought to be caused by abnormal glycosylation [15, 19]. PGs are composed of core proteins and one or more glycans with modifications. PGs are present in the extracellular matrix and have important diverse biological functions [5]. PG synthesis is initiated by the sequential addition of four monosaccharides (xylose [Xyl], two molecules of galactose [Gal] and glucuronic acid [GlcA]), known as a linker tetrasaccharide, to the serine residue of the core protein backbone (Fig. 10.1a). Additional sugar chains are extended from the linker tetrasaccharide by the addition of repeated disaccharides (usually consisting of 50–150 disaccharides in vivo). Afterwards, some sugars are modified by a series of epimerases (epimerization) and sulfotransferases (sulfation).

GAGs are long unbranched polysaccharides consisting of repeating disaccharide units. GAGs are highly negatively charged because of the acidic sugar residues and/or sulfation. Consequently, GAG can change its conformation, attract cations, and bind water. Hydrated GAG gels enable joints and tissues to absorb large pressure changes, providing tissue elasticity. Post-translational modifications such as epimerization, sulfation, and acetylation/deacetylation result in the formation of diverse motifs in the GAG chains, which can bind to a large variety of ligands. Therefore, GAG chains play important roles in regulating growth factor signaling, cell adhesion, proliferation, differentiation, and motility [3, 5, 45].

GAGs can be divided into two groups: (1) galactosaminoglycans such as chondroitin sulfate (CS) and dermatan sulfate (DS), and (2) glucosaminoglycans such as hyaluronic acid, keratan sulfate, heparan sulfate, and heparin [42]. Two types of glycosylation are known: *O*-glycosylation and *N*-glycosylation (Fig. 10.2a). Most GAGs (except for keratan sulfate and hyaluronic acid) are *O*-glycans that bind to the glycan via an oxygen molecule in the serine or threonine residue of the core protein (Fig. 10.2a). Notably, failure to add the first or second galactose residue of the tetrasaccharide results in the progeroid type of EDS (Fig. 10.1b, c).

The CS and DS GAGs are produced via the same pathway (Fig. 10.3a). In this pathway, after the linker tetrasaccharide attaches to the serine